An evolutionary-based inverse approach for the identification of non-linear heat generation rates in living tissues using a localized meshless method

Received 5 December 2006
Revised 25 May 2007
Accepted 25 May 2007

Kevin Erhart
Mechanical, Materials and Aerospace Engineering Department, University of Central Florida, Orlando, Florida, USA
Eduardo Divo
Department of Engineering Technology, University of Central Florida, Orlando, Florida, USA, and
Alain Kassab
Mechanical, Materials and Aerospace Engineering Department, University of Central Florida, Orlando, Florida, USA

Abstract

Purpose – This paper aims to develop and describe an improved process for determining the rate of heat generation in living tissue.

Design/methodology/approach – Previous work by the authors on solving the bioheat equation has been updated to include a new localized meshless method which will create a more robust and computationally efficient technique. Inclusion of this technique will allow for the solution of more complex and realistic geometries, which are typical of living tissue. Additionally, the unknown heat generation rates are found through genetic algorithm optimization.

Findings – The localized technique showed superior accuracy and significant savings in memory and processor time. The computational efficiency of the newly proposed meshless solver allows the optimization process to be carried to a higher level, leading to more accurate solutions for the inverse technique. Several example cases are presented to demonstrate these conclusions.

Research limitations/implications – This work includes only 2D development of the approach, while any realistic modeling for patient-specific cases would be inherently 3D. The extension to 3D, as well as studies to improve the technique by decreasing the sensitivity to measurement noise and to incorporate non-invasive measurement positioning, are under way.

Practical implications – As medical imaging continuously improves, such techniques may prove useful in patient diagonosis, as heat generation can be correlated to the presence of tumors, infections, or other conditions.

Originality/value – This paper describes a new application of meshless methods. Such methods are becoming attractive due to their decreased pre-processing requirements, especially for problems involving complex geometries (such as patient specific tissues), as well as optimization problems, where geometries may be constantly changing.

Keywords Optimization techniques, Heat transfer, Body systems and organs

Paper type Research paper

International Journal of Numerical Methods for Heat & Fluid Flow
Vol. 18 No. 3/4, 2008
pp. 401-414

0961-5539
DOI 10.1108/09615530810853655

Nomenclature

T	= field temperature	W_b	= blood perfusion term
k	= thermal conductivity	U_G	= total heat generation rate
ρ	= density	x,y	= spatial coordinates
c	= specific heat	r	= Euclidean distance
h_m	= rate of metabolic heat generation	α	= meshless expansion coefficients
h_b	= rate of heat generation due to blood perfusion	$\chi(r)$	= radial basis function (RBF)
		s	= RBF shape parameter
t	= time	$\mathbf{n}$	= outward normal vector
T_o	= arterial temperature	p	= current time level

1. Introduction

The Bioheat equation, which is a slight variation to the transient heat conduction equation, is typically used to model heat transfer in living tissue, particularly in human tissue. The form proposed by Pennes (1948) for the bioheat equation is as follows:

$$\rho c \frac{\partial T}{\partial t} = k\nabla^2 T + h_m + h_b \tag{1}$$

with h_m and h_b being heat generation rates from metabolic processes and blood perfusion within the tissue, respectively. The rate of heat generation by perfusion is typically found by the following expression:

$$h_b = W_b \rho_b c_b (T_o - T) \tag{2}$$

where, ρ_b and c_b are the blood density and specific heat, respectively, and W_b is the blood perfusion term. The total heat generation, U_G is therefore given by:

$$U_G(T) = h_m + W_b \rho_b c_b T_o - W_b \rho_b c_b T \tag{3}$$

where T_o is the constant arterial temperature. Jiji *et al.* (1984), Weinbaum and Jiji (1985) and Weinbaum *et al.* (1997) have offered several improvements to this basic equation over the years, which may better include the mechanism of counter-current heat exchange. Any deficiencies with Pennes' equation however, are not too substantial, as discussed by Wissler (1998), and much work in this area still uses the standard form of the bioheat equation as given by Pennes. The blood perfusion term, W_b, is often taken as a constant value that allows a specific model to closely match experimental data. Jiji *et al.* (1984) may have more correctly captured the true mechanism by which heat is exchanged, but the generality of the perfusion term allows the standard form of the bioheat equation, equation (1), to model the tissue heat transfer process quite well. This term is often unknown, thus modeling results in literature are often shown over a range of perfusion values (assuming this term is a constant). Since, this term is quite important to the bioheat equation, it would be quite useful to be able to predict its value precisely. From the equations above, and assuming a constant value for W_b, the total rate of heat generation should have a linear relationship with temperature. Assuming a linear relationship, $U_G(T) = a + bT$, where $b = -W_b \rho_b c_b$ and $a = h_m + W_b \rho_b c_b T_o$. Since, the heat generation rate coefficients, h_m and W_b, are unknown, an inverse type problem is encountered. This inverse problem can be solved if additional information other than the typical boundary conditions needed for the direct solution are provided. The additional information may be interior tissue temperature measurements, or simply redundant boundary information (specifying both temperature and flux at the boundary). Using this extra information an optimization process can be used for the determination of the blood perfusion rate as well as the value of metabolic heat

generation (assuming that the temperature of the arterial blood, T_o is known). However, the circulation of blood is one of the main temperature regulatory processes of the body, thus the blood perfusion term, W_b, should likely vary with tissue temperature. Therefore, the heat generation rate should be considered a function of tissue temperature. Liu and Xu (2000) use a linear form for W_b in their study using a transient boundary element technique, but to be more general here, a polynomial expression will be used for the variation of heat generation with temperature, given by:

$$U_G(T) = \sum_{i=0}^{N_U} a_i T^i \tag{4}$$

where, N_U is the order of the polynomial, and the α's are the coefficient values representing the variation of heat generation with temperature. It will be assumed that, the metabolic rate of heat generation is constant with respect to temperature (changes it this parameter over time are likely however, but will not be addressed here), and the perfusion term will be used to capture the variation of heat generation rate with tissue temperature.

2. Inverse problem solution using genetic algorithm optimization

Since, the rates of heat generation within the domain of interest are not known in this particular problem, it cannot be solved directly. In order to solve the problem directly, the heat generation rates must be assumed. The resulting solution field can then be checked against the known data to test the accuracy of the solution. This process must be repeated until an acceptable match of the solution field to the known data is obtained. The idea of using an optimization procedure for determining such unknowns, thus solving the inverse problem, is not new and is well discussed in literature. Since, this problem is nonlinear, a gradient-based optimization scheme may not produce the best possible results, due to the possible existence of local minima. In order to obtain a globally optimized solution a discrete genetic algorithm (GA), will be employed. GA have been shown to provide highly optimal solutions in numerous types of inverse problems (Han *et al.*, 2003; Pastorino *et al.*, 2002; Wu *et al.*, 2002; Divo *et al.*, 2004).

The discrete GA operates over a specified range or solution space, by discretizing the range using a set number of binary bits. The number of bits determines the resolution of the solution, and is a large factor in the rate of convergence of the procedure. The resolution is calculated through the simple relationship given below:

$$\text{Res} = \frac{\text{Range}}{2N\text{bit} - 1} \tag{5}$$

where Range is the size of the parameter search space and Nbit is the number of bits used for the parameter. A fixed population size (50) is employed in this application of the GA. The initial population is generated at random, where each individual consists of a number of binary values (8 bits used herein). Each set of binary values corresponds to one optimization parameter. Since, the goal of this work is to find the temperature dependent rate of heat generation, the optimization parameters have been chosen as the polynomial coefficients of the heat generation rates, in the form given by equation (4), where N_U is the pre-selected order of the polynomial and the α's are the coefficient values, which will be determined through the optimization process.

Once the GA has created a population of individuals, the fitness for each individual is calculated using the following expression:

$$\text{Fitness}_j = \sum_{i=1}^{\text{NIK}} |\text{TK}_i - \text{TI}(x_i, y_i)_j| \tag{6}$$

where NIK is the number of known interior temperature measurements, TK are the known interior temperatures, and $\text{TI}(x_i, y_i)_j$ are the temperatures computed from the direct solver for the jth individual. Individuals then reproduce in a probabilistic manner, based on their relative fitness value. This particular version of the GA uses a "kill" routine, which erases the current population and regenerates a new random population (the best individual is kept however), to ensure the GA does not stall in local minima and produces a globally optimal solution. A "creep" mutation parameter is also used to help the GA fine tune the solution once it has found an area of local minimization.

The evaluation of the fitness function for each individual requires a direct solver for the bioheat equation capable of handling the nonlinear generation term. The direct solver chosen for this work is a meshless collocation method. It is also noteworthy that the fitness of each individual is independent of the other individuals, therefore the problem is solved quite efficiently using a parallel computation scheme. This allows the fitness of multiple individuals to be evaluated simultaneously, significantly reducing the computational time needed for the optimization process. Also, since only the rate coefficients and fitness for each individual need to be passed to additional processors, (this communication time is very small compared to the amount of computational time required for each direct solution) the overall solution time scales quite linearly with the number of processors.

3. Localized meshless solver

The major focus of this work is the inclusion of a new localized meshless method solver for the bioheat equation. The initial development using the global meshless technique is given by the authors (Erhart *et al.*, 2005), and the details of the development of the localized technique is given by Divo and Kassab (2005a). Several verification examples are presented which demonstrate the accuracy and efficiency of the technique. The method is also implemented for heat transfer with solidification by Zaloznik *et al.* (2005). A major advantage of these so-called meshless methods is the ease of setup for a problem. No elaborate mesh or grid is needed, only a simple distribution of points. The localized technique requires the determination of an influence field, or topology, for each collocation point however. It may be argued that these topologies represent a type of mesh, thus making this technique not truly mesh free; the topologies however are easily generated automatically and solutions are much less sensitive to the topology configuration than to the element distribution in a FEM type solution. A typical meshless problem geometry along with a representative topology is shown in Figure 1. Such topologies are generated automatically by inclusion of all points within a certain radial distance, which is determined at run time such that a pre-defined number of points in each direction is included in each topology. The problem boundary conditions are satisfied at the boundary points, while the governing equation is satisfied at all interior points using a collocation technique.

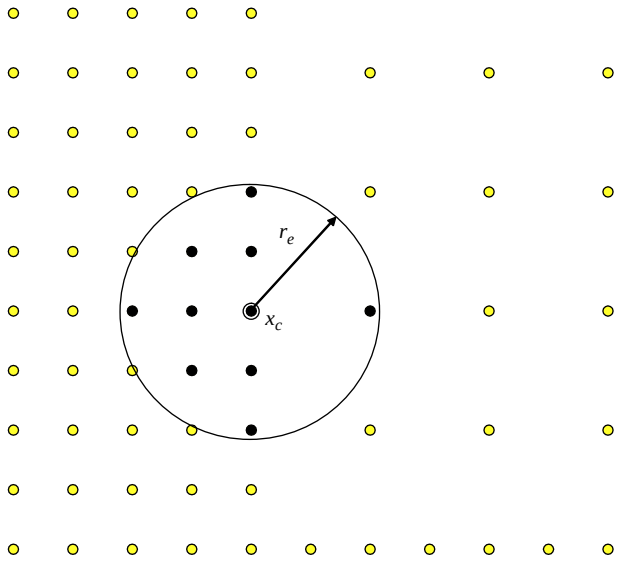

Figure 1.
Typical meshless problem geometry and topology

The meshless approximation is accomplished by locally expanding the temperature over a small number NTP of independent points. These points may by in the domain $\Omega(x, y)$ and/or on the boundary $\Gamma(x, y)$:

$$T(x,y,t) = \sum_{j=1}^{\mathrm{NF}} \alpha_j(t)\chi_j(x,y) + \sum_{j=1}^{\mathrm{NP}} \alpha_{j+\mathrm{NF}}(t)P_j(x) \tag{7}$$

where $\alpha_j(t)$ is the transient expansion coefficient, for the current topology, NF is the number of expansion functions while $\chi_j(x, y)$ denotes the expansion functions. An additional, NP, polynomial functions $P_j(x)$ are added to the expansion to guarantee that constant and linear fields can be retrieved by the expansion exactly. The multiquadric radial basis function (RBF) has been shown to accurately interpolate field variables by Kansa and Hon (2000) and has proved quite sufficient in other works by Divo and Kassab (2005b, 2006), and it is chosen as the expansion function in this work. The inverse multiquadric RBF used herein is defined as:

$$\chi_j(x,y) = \left[r_j^2(x,y) + c^2\right]^{-1/2} \tag{8}$$

where r_j is the Euclidean distance from (x, y) to (x_j, y_j), and c is the so-called shape parameter which is chosen based on the guidance provided by Cheng *et al.* (2003). The shape parameter c single-handedly dictates the behavior of, what is most important in the meshless model: the derivatives of the expansion. For a specific expansion over a specific set of data centers, the larger the shape parameter c, the smoother the derivative field. However, the magnitude of the shape parameter c cannot be increased without bound, as the expansion functions become flatter, and hence, the coefficient matrix resulting of the collocation over data centers becomes ill-conditioned. For this reason, a simple optimization search is employed to determine every value for the shape parameter c used in every expansion over the different local topologies that cover the entire field. An initial guess for c is based on the ratio of the average distance

between data centers in a topology to the number of points in the topology. A GA is utilized to optimize the shape parameter value for each data center such that the conditioning number of the interpolant matrix is as high as possible without degrading the accuracy of the solution.

A forward difference approximation is now applied to estimate the time derivative term in the bioheat equation, equation (1) above, resulting in the following expression:

$$k\nabla^2 T^{(p)} + h_{\mathrm{m}}^{(p)} + h_{\mathrm{b}}^{(p)} = \rho C \frac{T^{(p+1)} - T^{(p)}}{\Delta t} \tag{9}$$

where p represents the time step. This expression is easily solved for the temperature at the next time step, $T^{(p+1)}$, which yields:

$$T^{(p+1)} = \frac{\Delta t}{\rho C}\left[k\nabla^2 T^{(p)} + h_{\mathrm{m}}^{(p)} + h_{\mathrm{b}}^{(p)}\right] + T^{(p)} \tag{10}$$

The Laplacian term in this expression is found from the previous time step temperatures using the RBF expansion above.

The real advantage of the localized collocation approach is a consequence of manner in which the derivatives at the center of the topology are calculated (Divo and Kassab, 2005c, 2007). The collocation of the known (from previous time level) temperature, T, for instance, at the points within the localized topology, leads to the following in matrix-vector form:

$$\{\mathbf{T}\} = [\mathbf{C}]\{\alpha\} \Rightarrow \{\alpha\} = [\mathbf{C}]^{-1}\{\mathbf{T}\} \tag{11}$$

The interpolation matrix $[\mathbf{C}]$ and the vector $\{\mathbf{T}\}$ are given by:

$$[\mathbf{C}] = \begin{bmatrix} \chi_1(x_1) & \cdots & \chi_{\mathrm{NF}}(x_1) & P_1(x_1) & \cdots & P_{\mathrm{NP}}(x_1) \\ \vdots & & \vdots & \vdots & & \vdots \\ \chi_1(x_{\mathrm{NF}}) & \cdots & \chi_{\mathrm{NF}}(x_{\mathrm{NF}}) & P_1(x_{\mathrm{NF}}) & \cdots & P_{\mathrm{NP}}(x_{\mathrm{NF}}) \\ P_1(x_1) & \cdots & P_1(x_{\mathrm{NF}}) & 0 & \cdots & 0 \\ \vdots & & \vdots & \vdots & & \vdots \\ P_{\mathrm{NP}}(x_1) & \cdots & P_{\mathrm{NP}}(x_{\mathrm{NF}}) & 0 & \cdots & 0 \end{bmatrix}, \{\mathbf{T}\} = \begin{pmatrix} T(x_1) \\ \vdots \\ T(x_{\mathrm{NF}}) \\ 0 \\ \vdots \\ 0 \end{pmatrix} \tag{12}$$

Then, to estimate the field variable derivatives at the data center, the linear Laplacian differential operator $\mathscr{L}$ is applied to the localized expansion equation as:

$$\mathscr{L}T(x_{\mathrm{c}}) = \sum_{j=1}^{\mathrm{NF}} \alpha_j \mathscr{L}\chi_j(x_{\mathrm{c}}) + \sum_{j=1}^{\mathrm{NP}} \alpha_{j+\mathrm{NF}} \mathscr{L}P_i(x_{\mathrm{c}}) \tag{13}$$

where, x_{c} is the data center of the topology. Thus, in matrix-vector form:

$$\mathscr{L}T_{\mathrm{c}} = \{\mathscr{L}_{\mathrm{c}}\}^T\{\alpha\} \Rightarrow \mathscr{L}T_{\mathrm{c}} = \{\mathscr{L}_{\mathrm{c}}\}^T[\mathbf{C}]^{-1}\{\mathbf{T}\} \Rightarrow \mathscr{L}T_{\mathrm{c}} = \{\mathscr{L}_{\mathrm{c}}\}^T\{\mathbf{T}\} \tag{14}$$

with the vector $\{\mathscr{L}_c\}$ composed by:

$$\{\mathscr{L}_c\}\begin{pmatrix} \mathscr{L}\chi_1(x_c) \\ \vdots \\ \mathscr{L}\chi_{NF}(x_c) \\ \mathscr{L}P_1(x_c) \\ \vdots \\ \mathscr{L}P_{NP}(x_c) \end{pmatrix} \tag{15}$$

Therefore, evaluation of the field variable derivatives at everyone of the data centers x_c is provided by a simple inner product of two small vectors: $\{\mathscr{L}_c\}$ which can be pre-built and stored and $\{\mathbf{T}\}$ which is the updated field variable around the topology of the data center x_c.

In addition, when imposing the generalized boundary condition at the boundary data centers, the derivative expansion can be easily implemented to retrieve the value of the temperature. In particular, imposing a Robin condition that can be specialized to Dirichlet or Neumann:

$$\eta\frac{\partial T}{\partial n} + \gamma T = \beta \tag{16}$$

Then, introducing the expansion for the derivatives yields:

$$\eta\{\partial n\}^T + \{\mathbf{T}\} + \gamma T = \beta \tag{17}$$

Then, the value of the field variable T_c at the data center x_c of the topology can be retrieved directly by re-arranging the equation above as:

$$T_c = \{\mathbf{\Gamma}\}^T\{\boldsymbol{\lambda}\} \tag{18}$$

Where the vector $\{\mathbf{\Gamma}\}$ contains the interpolation information and boundary condition parameters and therefore can be pre-build at setup stage, while the vector $\{\boldsymbol{\lambda}\}$ contains the boundary condition value and temeprature values inside the topology excluding the topology center. Hence, the feature of the localized method of being able to retrieve the temperature and its derivatives by simple vector-vector products is preserved.

The particular feature of the localized collocation method that allows the estimate of the field variables and their derivatives by simple inner products of vectors (that can be pre-built and stored) is precisely what makes this approach efficient. The multiquadric functions need only be evaluated at a setup stage when these vectors are being built, reducing the CPU burden of having to evaluate fractional powers and complicated functions at every step of an iteration or time-marching scheme. In addition, the memory demands of this approach are minimal, as no global collocation matrix is allocated, and only very small vectors are stored for every data center. The local RBF method thus offers termendous computational advantages in terms of data preparation over global RBF meshless methods. As such, local meshless RBF is adopted as the solution method for the inverse problem considered in this paper, while results from a global RBF inverse method are reported as well for comparison.

4. Numerical examples

Since, the methodology used for the determination of the heat generation has been verified by the previous use of the global meshless method by the authors, the first example below will demonstrate the efficiency and accuracy improvements of employing the new localized meshless technique. For this first problem the blood perfusion term, W_b, was assumed to have a quadratic relationship with tissue temperature of the form:

$$W_b(T) = W_{b_0} + W_{b_1} T + W_{b_2} T^2 \tag{19}$$

Figure 2 shows the geometric setup of this verification problem, including the measurement locations. Table I provides a list of all the necessary properties for this problem, and some additional properties which will be used in later problems. The boundary conditions employed are convection at the skin surface ($T\infty = 300\,\mathrm{K}$, $h = 5\,\mathrm{W/m^2K}$), and fixed temperatures at all other surfaces. We used a linear interpolation of temperatures measured experimentally by Pennes (1948), who utilized a thin wire thermocouple embedded in live human subject forearms. The problem is time marched to steady from an arbitrary initial condition in all cases. It is understood that such boundary conditions are not easily obtained in a realistic situation, so this problem is being used as a proof of concept until a realistic 3D model can be developed and appropriate boundary conditions imposed.

Figure 3 shows the temperature field solution for the known case (direct solution using the chosen rate coefficients shown in Table II) and the inverse solution case for the new local method. Additionally, the rate coefficients for both the global method and the new local method are displayed in Table II. The similarities in the solution fields shows that the local method also produces comparable results. Most noteworthy with

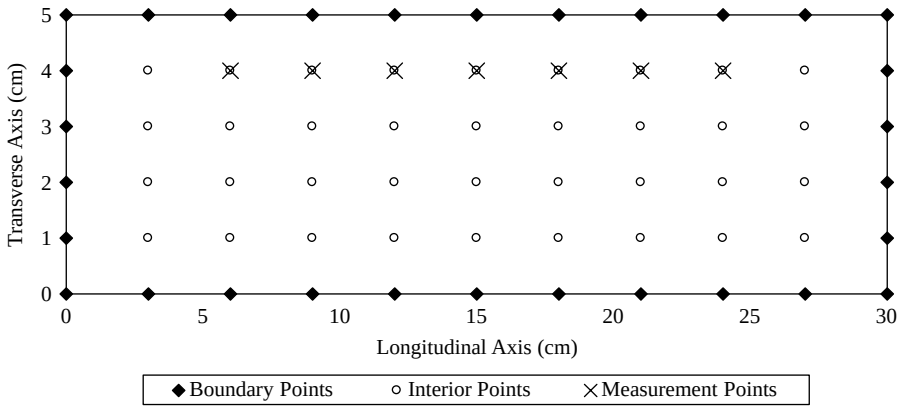

Figure 2.
Geometry of verification problem

Material	Density (kg/m^3)	Specific heat (J/kg K)	Conductivity (W/m K)
Tissue	1,050	3,800	0.510
Bone	1,800	1,250	0.867

Sources: Jiji *et al.* (1984) and Weinbaum *et al.* (1997)

Table I.
Material properties used for example problems

these results is the computational time for the new method. For a single direct field solution for this problem, the previous global method required 42.1 s, while the new local method required only 0.234 s. This is a tremendous improvement in computational efficiency for the new local meshless technique, bringing the performance of the meshless method to the level of FEM and Finite Differencing in terms of solution speed. Figure 4 shows a plot of the temperature dependent heat generation rates for the chosen rate coefficient values as well as the inverse calculated

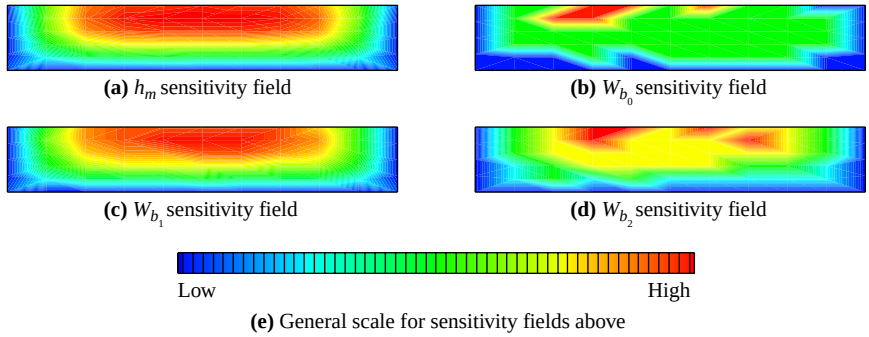

(a) h_m sensitivity field

(b) W_{b_0} sensitivity field

(c) W_{b_1} sensitivity field

(d) W_{b_2} sensitivity field

(e) General scale for sensitivity fields above

Figure 3.
Sensitivity fields for each heat generation rate coefficient

	Known values	Global inverse predicted values	Local inverse predicted values
a_0	440.00	449.02	447.06
a_1	−0.045	−0.02627	−0.07678
a_2	−0.0015	0.0000392	−0.001373
a_3	−0.0000012	−0.00000671	−0.00000153

Table II.
Assumed and calculated heat generation rate coefficients for initial example problem

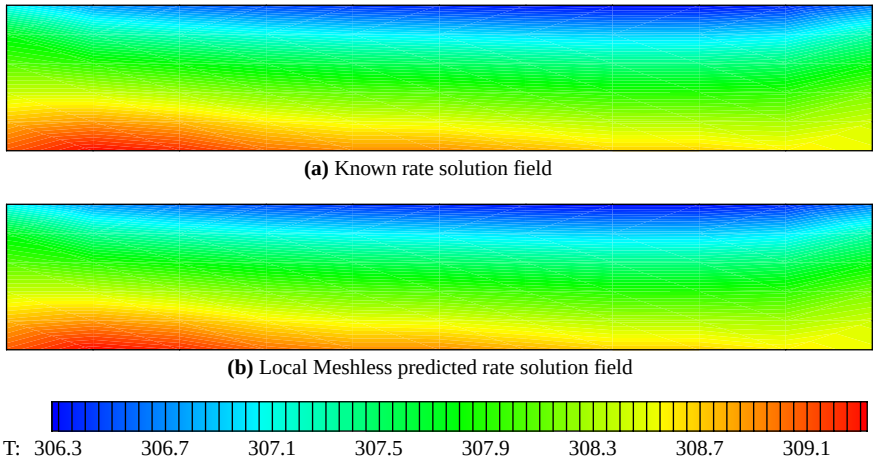

(a) Known rate solution field

(b) Local Meshless predicted rate solution field

(c) Temperature scale for both fields

Figure 4.
Known and predicted (from inverse solution) temperature fields for initial verification problem

(predicted) values, plotted over the temperature range for this verification example. There does appear to be some difference in the curves for the previous global method, but the local method produces even more comparable results. It should be noted that the maximum generation rate error for the local method does not exceed 0.05 percent of the total rate within the range of temperatures present, showing that the results are very accurate. It should be noted that the location of the sensors is typically guided by a sensitivity analysis (Erhart *et al.*, 2005; Majchrzak and Mochnacki, 2006) to determine the most appropriate placement of the interior measurements. Measurement locations are sought such that the sensitivites there are far from zero and measurements are physically possible. For example, the sensitivity maps for the variables of interest for the first problem are shown in Figure 5.

Now that some confidence has been gained in the local technique, a more complex problem can be analyzed. Figure 6 shows the geometry that will be used for the next example problem. This problem is similar to the first case above, but now includes a region of bone, making the problem non-homogeneous (Table I above for the properties used for bone). Blood perfusion through the bone is likely not as prevalent as in

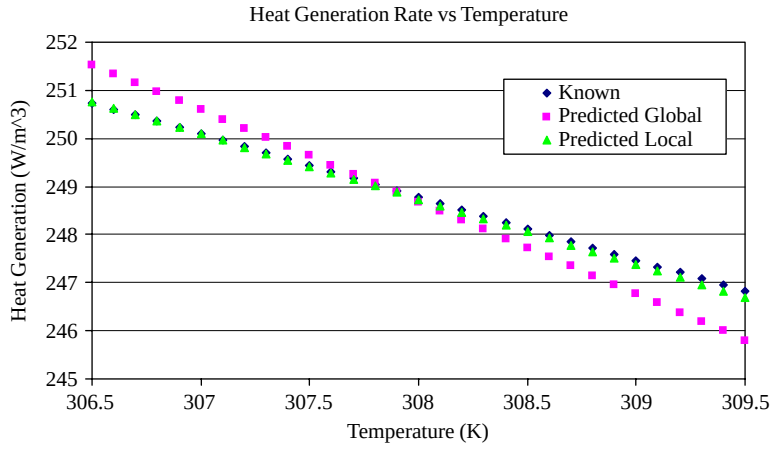

Figure 5.
Plot of generation rate vs temperature for known and predicted rate coefficients

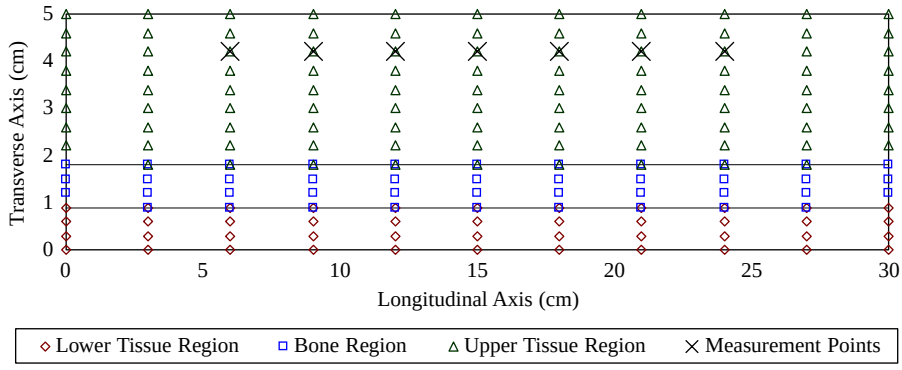

Figure 6.
Geometry of example problem with bone and tissue regions

the tissue, and little metabolic generation occurs in bone, thus the heat generation in this area can be assumed negligible by comparison. This example may provide some insight into the effects of the presence of bone on heat transfer rates.

Similar results are presented below for this problem. Figure 7 compares the known generation function to the predicted for both the global and local methods. For both methods all rates fall within 1 percent of the total rate over the temperature range of interest, but the new local method is easily seen to provide more accurate results. Figure 8 shows the entire temperature fields obtained for both the known and the predicted generation rate coefficients using the local method. Very close agreement is again obtained throughout the entire field. Figure 9 shows the residual error between the predicted temperatures and the known temperatures at the measurement locations (for the best individual) throughout the entire GA optimization process.

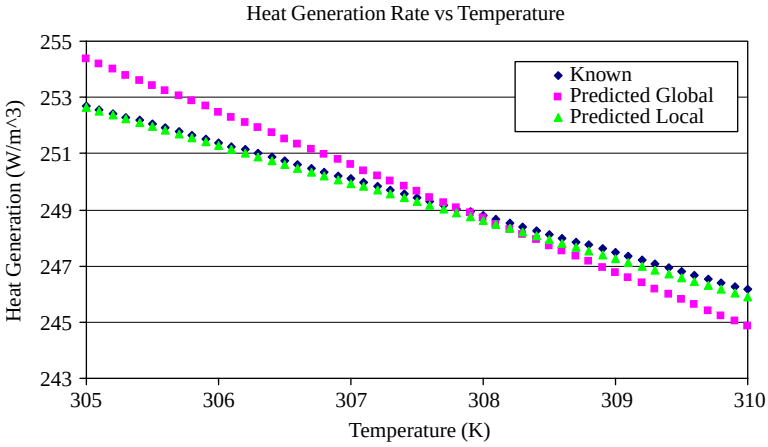

Figure 7.
Plot of heat generation rate vs temperature for known and predicted heat generation rates

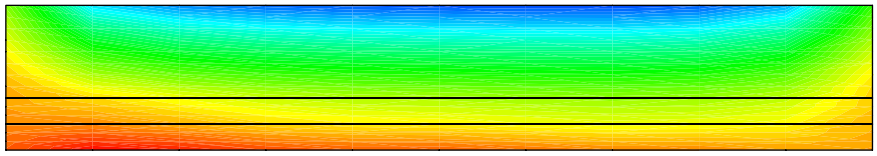

(a) Known rate solution field

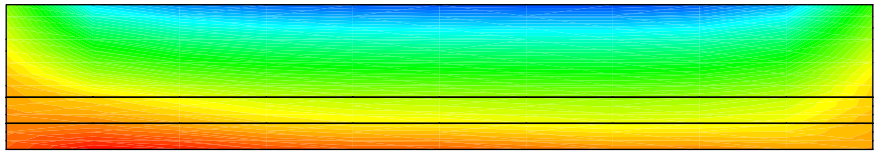

(b) Local Meshless predicted rate solution field

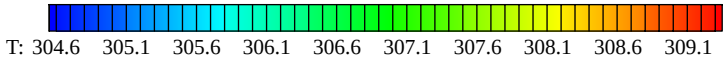

(c) Temperature scale for both fields

Figure 8.
Known and predicted temperature fields for example with addition of bone region

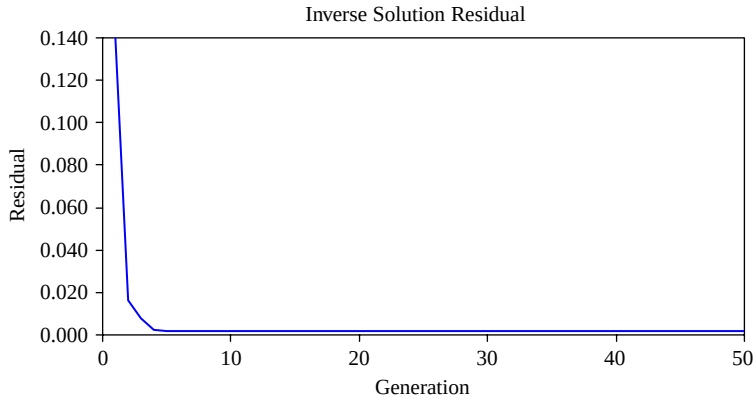

Figure 9.
Temperature difference residual vs generation in genetic algorithm

Now that confidence has been gained that the local meshless method and the inverse methodology used herein can produce accurate rate predictions, we can investigate further by adding some random error to our simulated measurement data. Measurement error would always exist in this type of analysis so it is important that this technique is capable of producing acceptable results even with such errors present. Two such trials were performed using the geometry and boundary conditions for the first problem described above (tissue only case). In one case a random error of ± 0.1 K maximum was added to the simulated measurement data at all measurement locations. In the second case an error of ± 0.25 K was added. The resulting rate predictions are shown in Figure 10. At first glance it may appear that the results for these cases are not acceptable, however if one looks at the percent error for each case, it is seen that the rates are predicted within 5 percent for the first case and 9 percent for the second case. For many cases this level of accuracy would be sufficient.

5. Summary

Improvements in efficiency in the meshless collocation solver using a new localized approach have been presented. An inverse solution procedure using a discrete GA,

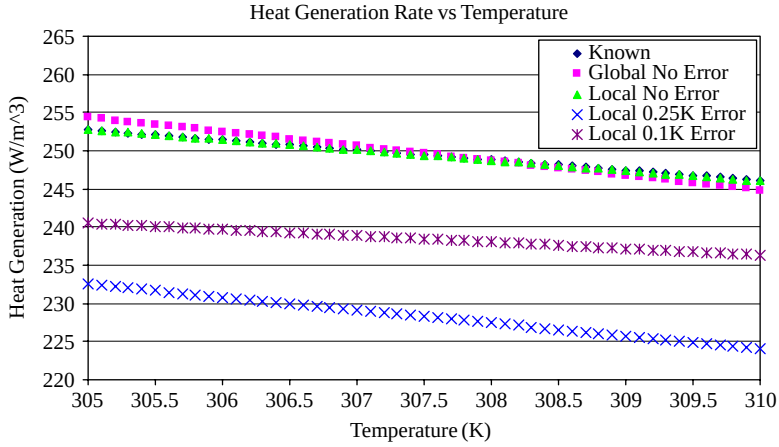

Figure 10.
Plot of heat generation rate vs temperature for cases with simulated measurement noise

coupled with this meshless solver have been used for determining the unknown blood perfusion rate and the metabolic rate of heat generation in living tissue (the bioheat equation). Two examples have been shown which demonstrate the vast efficiency improvements of this approach, and provide quantitative measurements of its accuracy and effectiveness. Additionally, the effects of measurement noise have been quantified for a simple case, and while the results are not perfect, they are within an acceptable range for most engineering applications. Additional test cases are currently under consideration to test for possible improvements and determine the effectiveness for more complex geometries with measurement noise. Further investigations using this technique will also include the use of boundary only data (avoiding the need for invasive measurements), the extension to 3D, as well as the inclusion of spatial, temporal, and temperature tissue property variation.

References

Cheng, A.H-D., Golberg, M.A., Kansa, E.J. and Zammito, G. (2003), "Exponential convergence and H-c multiquadric collocation method for partial differential equations", *Numerical Methods in P.D.E.*, Vol. 19 No. 5, pp. 571-94.

Divo, E. and Kassab, A.J. (2005a), "An efficient localized RBF meshless method applied to fluid flow and conjugate heat transfer", ASME Paper IMECE2005-82150.

Divo, E. and Kassab, A.J. (2005b), "A meshless method for conjugate heat transfer", in Papadrakakis *et al.* (Eds), *Proceedings of ECCOMAS 2005, International Conference on Computational Methods for Coupled Problems in Science and Engineering, Santorini, May 25-28*.

Divo, E. and Kassab, A.J. (2005c), "Modeling of convective and conjugate heat transfer by a third order localized RBF meshless collocation method", in Bialecki, R.A. and Nowak, A.J. (Eds), *Proceedings of NHT-05 Eurotherm82*, pp. 357-66.

Divo, E. and Kassab, A.J. (2006), "Iterative domain decomposition meshless method modeling of incompressible viscous flows and conjugate heat transfer", *Engineering Analysis with Boundary Elements*, Vol. 30 No. 6, pp. 465-78.

Divo, E. and Kassab, A.J. (2007), "An efficient localized RBF meshless method for fluid flow and conjugate heat transfer", *ASME Journal of Heat Transfer*, Vol. 129, pp. 124-36.

Divo, E., Kassab, A.J. and Rodriguez, F. (2004), "A hybrid singularity superposition/BEM method for the solution of the inverse geometric problem", *Numerical Heat Transfer, Part B: Fundamentals*, Vol. 46, pp. 1-30.

Erhart, K., Divo, E. and Kassab, A.J. (2005), "An inverse meshless technique for the determination of non-linear heat generation rates in living tissue", in Bialecki, R.A. and Nowak, A.J. (Eds), *Proc. of NHT-05 Eurotherm82*, pp. 483-92.

Han, H., Zhang, Z. and Wei, P. (2003), "Genetic algorithm for parameter inversion of saturated porous media", *Journal of Rock Mechanics and Engineering*, Vol. 22 No. 9, pp. 1458-62.

Jiji, L.M., Weinbaum, S. and Lemons, D.E. (1984), "Theory and experiment for the effect of vascular microstructure on surface tissue heat transfer – Part II: model formulation and solution", *Journal of Biomechanical Engineering*, Vol. 106, pp. 331-41.

Kansa, E.J. and Hon, Y.C. (2000), "Circumventing the Ill-conditioning problem with multiquadric radial basis functions: applications to elliptic partial differential equations", *Comp. Math. Appl.*, Vol. 39, pp. 123-37.

Liu, J. and Xu, X. (2000), "Boundary information based diagnostics on the thermal states of biological bodies", *International Journal of Heat and Mass Transfer*, Vol. 43, pp. 2827-39.

Majchrzak, E. and Mochnacki, B. (2006), "Sensitivity analysis and inverse problems in bio-heat transfer modelling", *Computer Assisted Mechanics and Engineering Sciences*, Vol. 13 No. 1, pp. 85-108.

Pastorino, M., Caorsi, S. and Massa, A. (2002), "A global optimization technique for microwave nondestructive evaluation", *IEEE Transactions on Instrumentation and Measurement*, Vol. 51 No. 4, pp. 666-73.

Pennes, H. (1948), "Analysis of tissue and arterial blood temperature in the resting forearm", *Journal of Applied Physiology*, Vol. 1, pp. 93-122.

Weinbaum, S. and Jiji, L.M. (1985), "A new simplified bioheat equation for the effect of blood flow on local average tissue temperature", *J. of Biomech. Eng.*, Vol. 107, pp. 131-9.

Weinbaum, S., Xu, L.X., Zhu, L. and Ekpene, A. (1997), "A new fundamental bioheat equation for muscle tissue: Part I – blood perfusion term", *J. of Biomech. Eng.*, Vol. 119, pp. 278-88.

Wissler, E.H. (1998), "Pennes' 1948 paper revisited, 50 years of JAP", *American Physiological Society*, Vol. 85 No. 1, pp. 35-41.

Wu, Z.P., Liu, G.R. and Han, X. (2002), "An inverse procedure for crack detection in anisotropic laminated plates using elastic waves", *Engineering with Computers*, Vol. 18 No. 2, pp. 116-23.

Zaloznik, M., Xin, S. and Sarler, B. (2005), "Verification of a numerical model of microsegregation in direct chill casting", in Bialecki, R.A. and Nowak, A.J. (Eds), *Proceedings of NHT-05 Eurotherm82*, pp. 345-55.

Corresponding author
Alain Kassab can be contacted at: kassab@mail.ucf.edu